RF *p*-GaN HEMT With 0.9-dB Noise Figure and 12.8-dB Associated Gain for LNA Applications

Junmin Zhou, Haowen Guo, Haitao Du, Yu Zhang, Haolan Qu, Wei Huang, *Member, IEEE*, Jianjun Zhou, Zhiqiang Xiao, and Xinbo Zou, *Member, IEEE*

***Abstract*— Low-noise amplification performance of an enhancement-mode *p*-GaN gate high electron mobility transistor (HEMT) is thoroughly investigated. Featuring a tungsten (W) gate metal and CMOS-compatible metal contacts to source/drain terminals, the device exhibits a positive threshold voltage of 2.7 V. Low gate leakage current density (I_G) of 3.8 pA/mm and 16.3 nA/mm are extracted in pinch-off region and on-state region, respectively. The device delivers an input third-order interception point (IIP3) of 15.8 dBm at 2 GHz, together with good immunity of linearity characteristics against frequency change. A minimum noise figure (NF_{min}) of 0.9 dB with an associated gain (G_a) of 12.8 dB are achieved at a working frequency of 2 GHz. Furthermore, an examination of the bias and frequency effects on NF_{min} and G_a reveals NF_{min} of 0.65 dB and G_a of 18.3 dB at 1 GHz. This work paves a solid path for the utilization of *p*-GaN HEMT for low noise amplifier applications.**

***Index Terms*— Enhancement-mode, gate leakage, HEMT, linearity, noise figure, *p*-GaN gate, RF low noise amplifier.**

I. Introduction

GaN based high electron mobility transistors (HEMTs) have been used extensively in high-power and high-frequency applications [1], [2], [3], [4], owing to superior material properties including large critical electrical field, high carrier mobility in two dimensional electron gas (2-DEG), and good thermal conductivity [5], [6]. Recently, enhancement-mode (E-mode) HEMTs with *p*-GaN gates, which permit fail-safe operation and single-polarity bias design, have garnered considerable research interest for radio frequency (RF) applications. For instance, *p*-GaN HEMT with a gate-all-around structure has been successfully fabricated to deliver small-signal cutoff frequencies (f_T/f_{MAX}) of 6.0/9.8 GHz with a gate length (L_G) of 1 μm [7]. RF power amplifier (PA) performance of *p*-GaN HEMT, including a power added efficiency of 55% and output power density of 1.4 W/mm, has also been reported [8]. However, so far little information has emerged regarding the utilization of *p*-GaN HEMTs for low-noise amplifiers (LNAs), which represent essential components in RF front-end receivers. To meet the criterion of low noise figure (NF) in the receiver, which is typically dominated by the noise performance of LNA, gate leakage current (I_G) of LNA constituent device should be well suppressed [9]. To date, I_G in *p*-GaN HEMT has been reduced progressively, *e.g.,* by low work function metal gate contacts [10], or the usage of fluorinated graphene gate insertion layer [11], making *p*-GaN HEMT a potentially promising candidate for LNA applications.

In this contribution, we report low-noise amplification performance of an E-mode *p*-GaN HEMT, which featured a low I_G and CMOS-compatible Au-free metal scheme for ohmic contacts. RF low-noise amplifying characteristics of the *p*-GaN HEMT, including input third-order interception point (IIP3), NF, and associated gain (G_a), are thoroughly investigated for the first time. The results lay a solid foundation for the utilization of *p*-GaN HEMTs for implementing LNAs.

II. DC Performance of p-GaN HEMT

The E-mode HEMT used in this work [Fig. 1] consists of a 75 nm *p*-GaN cap layer, a 25 nm AlGaN barrier layer, a 300 nm GaN intrinsic layer, and a 4 μm GaN buffer. The gate electrode utilized low work function metal tungsten (W) to achieve Schottky contact with low gate leakage current. *P*-GaN layer in the source/drain regions were etched, followed by Tetramethylammonium Hydroxide (TMAH) and nitrogen plasma treatments. Source/drain ohmic contacts employed CMOS-compatible Au-free Ti/Al/Ti metal stack, which was annealed at 550 °C for 300 s in nitrogen. After depositing Al_2O_3/SiON passivation bi-layer, boron implantation was conducted to isolate the devices. The *p*-GaN HEMT also

Manuscript received 11 April 2023; revised 2 July 2023; accepted 10 July 2023. Date of publication 12 July 2023; date of current version 25 August 2023. This work was supported in part by ShanghaiTech University Startup Fund under Grant 2017F0203-000-14, in part by the National Natural Science Foundation of China under Grant 52131303, in part by the Natural Science Foundation of Shanghai under Grant 22ZR1442300, and in part by the Chinese Academy of Sciences (CAS) Strategic Science and Technology Program under Grant XDA18000000. The review of this letter was arranged by Editor S. Chowdhury. *(Corresponding author: Xinbo Zou.)*

Junmin Zhou, Haitao Du, Yu Zhang, and Haolan Qu are with the School of Information Science and Technology (SIST), ShanghaiTech University, Shanghai 201210, China, also with the School of Microelectronics, University of Chinese Academy of Sciences, Beijing 100049, China, and also with the Shanghai Institute of Microsystem and Information Technology, Shanghai 200050, China.

Haowen Guo and Xinbo Zou are with the School of Information Science and Technology (SIST), ShanghaiTech University, Shanghai 201210, China (e-mail: zouxb@shanghaitech.edu.cn).

Wei Huang is with the School of Microelectronics, Fudan University, Shanghai 200433, China.

Jianjun Zhou is with the Science and Technology on Monolithic Integrated Circuits and Modules Laboratory, Nanjing Electronic Devices Institute, Nanjing 211100, China.

Zhiqiang Xiao is with the Wuxi Microelectronics Scientific Research Center, Wuxi 214035, China.

Color versions of one or more figures in this letter are available at https://doi.org/10.1109/LED.2023.3294696.

Digital Object Identifier 10.1109/LED.2023.3294696

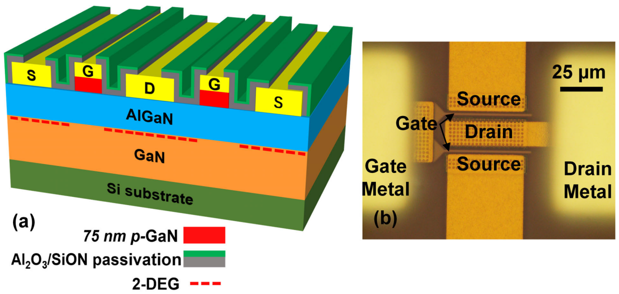

Fig. 1. (a) Schematic and (b) microscopic photograph of the *p*-GaN HEMT.

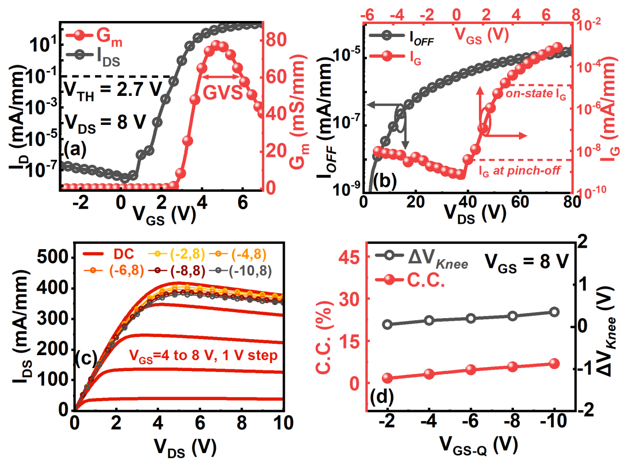

Fig. 2. (a) Transfer characteristics of the *p*-GaN HEMT (b) V_{GS} dependent I_G at $V_{DS} = 8$ V, and the I_{OFF} -V_{DS} characteristics at $V_{GS} = 0$ V. (c) DC output curve, and the pulsed I_{DS}-V_{DS} with various quiescent stress voltages ($V_{GS\text{-}Q}$, $V_{DS\text{-}Q}$) of *p*-GaN HEMT from (−2, 8) V to (−10, 8) V. (d) Quantitative current collapse and knee-voltage walkout.

features an L_G of 1 μm, a gate width of 2 × 50 μm, and gate-to-source/gate-to-drain lengths of 1.2 μm/1.65 μm.

Fig. 2(a) depicts transfer characteristics of the *p*-GaN HEMT. The device delivered a V_{TH} of 2.7 V (defined at 0.1 mA/mm) at V_{DS} = 8 V. Peak transconductance (G_m) of 78 mS/mm was obtained with V_{GS} = 5 V. Fig. 2(b) displays I_G and the off-state drain leakage current (I_{OFF}) characteristics of the device. I_G of only 3.8 pA/mm was achieved in pinch-off region (V_{GS} =1 V). On-state I_G was extracted to be 16.3 nA/mm at I_{DS} = 10 mA/mm (V_{GS} = 3.5 V), which was much smaller than previously reported conventional AlGaN/GaN HEMTs [9], [12]. The device also featured a low I_{OFF} of only 16 nA/mm at V_{GS}/V_{DS} = 0/80 V, demonstrating a breakdown voltage much larger than 80 V using the standard of $I_{OFF-Breakdown}$ =1 μA/mm.

Fig. 2(c) shows the output DC characteristics of the device with V_{GS} varying from 4 V to 8 V. The maximum I_{DS} was determined to be 417 mA/mm at V_{GS} = 8 V. Dynamic performance (V_{GS} = 8 V) of the device was measured employing various off-state quiescent stresses (V_{GS-Q}, V_{DS-Q}) with a pulse width of 5 ms and a period of 100 ms. Current collapse (C.C.), defined as $(1 - I_{sat.stress}/I_{sat.fresh}) \times 100\%$, and knee-voltage walkout (ΔV_{Knee}) are illustrated in Fig. 2(d). The pulsed I-V output results show that the device exhibited limited C.C., from 1.6% ($V_{GS-Q} = -2$ V) to 6.8% ($V_{GS-Q} = -10$ V). Also, ΔV_{Knee} of only 0.35 V at $V_{GS-Q} = -10$ V was achieved. The small C.C. and ΔV_{Knee} demonstrate that trapping and de-trapping processes in the device are well restrained, which is advantageous for the device to have good RF performance at relatively large input power [13], [14].

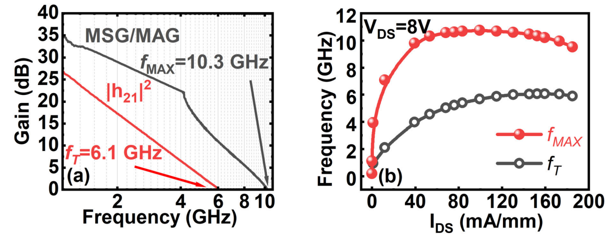

Fig. 3. (a) MSG/MAG and $|h_{21}|^2$ of *p*-GaN gate HEMT at $V_{GS} = 5$ V and $V_{DS} = 8$ V. (b) I_{DS} dependent f_T and f_{MAX}.

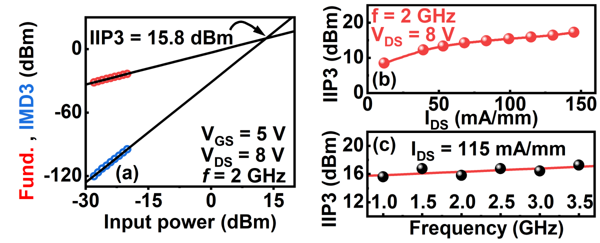

Fig. 4. (a) IIP3 of *p*-GaN HEMT (b) I_{DS} dependent IIP3 and (c) frequency dependent IIP3 of the device.

III. RF Performance of p-GaN HEMT

Fig. 3(a) reports the small-signal short-circuit current gain ($|h_{21}|^2$) and maximum stable gain/maximum available power gain (MSG/MAG) when the device was biased at V_{GS}/V_{DS} = 5/8 V, namely the peak G_m point (PGP). The current-gain cutoff frequency (f_T) and power-gain cutoff frequency (f_{MAX}) were extracted to be 6.1 GHz and 10.3 GHz, respectively. As shown in Fig. 3(b), both f_T and f_{MAX} exhibit rapid increases with increasing I_{DS} and then get saturated when I_{DS} exceeds 40 mA/mm. Also, f_T/f_{MAX} sustain above 80% of their maximum value over a wide range of I_{DS}, from 50 mA/mm to 185 mA/mm.

Fig. 4 illustrates the linearity characteristics of the device. Two-tone IIP3 measurement was performed with an offset frequency of 10 MHz. Fig. 4(a) shows the measured fundamental signal (Fund.) and third-order intermodulation (IMD3) components at a center frequency of 2 GHz while the *p*-GaN HEMT was biased at PGP. Small-signal input power of each tone was swept from −28 dBm to −20 dBm to keep the device working in its linear region. The IIP3 was extracted to be 15.8 dBm accordingly, and was attributed to the wide gate voltage swing (GVS, shown in Fig. 2(a)) of 2.1 V, which is defined as the maximum swing of gate voltage where G_m remains at or above 80% of its maximum value [15]. Fig. 4(b) reports the I_{DS} dependent IIP3. The IIP3 increases monotonically as increasing I_{DS}, from 8.5 dBm (I_{DS} = 10 mA/mm) to 17.3 dBm (I_{DS} = 150 mA/mm), which offers a wide bias-range selection for circuit design. The increase in bias-dependent IIP3 can be attributed to the fact that as increasing I_{DS}, the operating state of the device progressively shifts from deep Class AB to Class A, which is known for its higher linearity compared to devices operating in Class AB. Moreover, as shown in Fig. 4(c), IIP3 was determined to be 16 ± 1 dBm at various frequencies, demonstrating good frequency immunity of the device linearity characteristics.

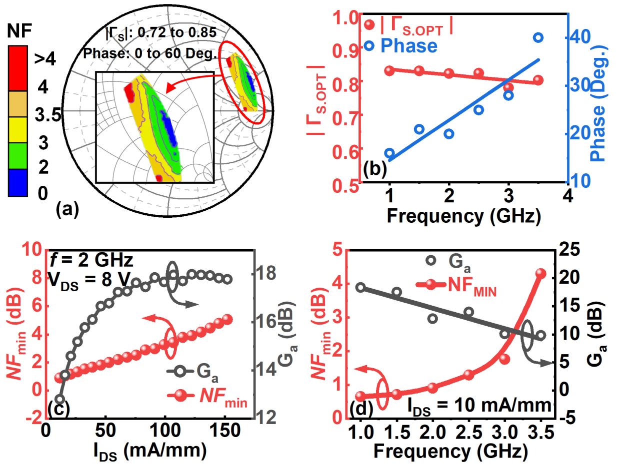

Fig. 5. (a) Measured NF with various Γ_S, (b) $|\Gamma_{S.OPT}|$ and phase versus frequency. NF_{min} and G_a as a function of (c) drain current and (d) working frequency.

Y-factor method was used as the NF measurement methodology [16]. In order to achieve the maximum signal gain, a load tuner was employed to conjugate match the output of device. Concurrently, a source tuner was adjusted to find the optimal source impedance of *p*-GaN HEMT where the device demonstrated the lowest NF. Fig. 5(a) depicts the measured NF with various source reflection coefficients (Γ_S) at 2 GHz (I_{DS} = 40 mA/mm), and the corresponding load impedance is set to be 232.5 + j296.27 Ω. NF reached its minimum value (NF_{min}) of 1.65 dB when Γ_S was tuned to $0.83\angle 20^\circ$ (corresponding to a source impedance of 124.14 + j219.18 Ω), and G_a was extracted to be 16.1 dB. Fig. 5(b) displays optimal source noise reflection coefficient $|\Gamma_{S.OPT}|$ and its phase angle as a function of frequency. As increasing frequency, $|\Gamma_{S.OPT}|$ shows a decreasing trend, while the phase angle increases from 16° to 40° conversely. The corresponding magnitude and phase of optimal load reflection coefficient (Γ_{Load}) decrease from 0.86 to 0.81 and increase from 7.5° to 22.4° (not shown in the figure), respectively. The increase in phase angle and the decrease in magnitude of reflection coefficients are due to the capacitive input/output impedances of the device, which would exhibit reduced capacitive reactance and smaller standing wave ratio (SWR) at higher frequencies.

Fig. 5(c) illustrates drain current dependent NF_{min} and G_a. NF_{min} increases monotonically as increasing I_{DS}, from only 0.90 dB (at 10 mA/mm) to 5.06 dB (at 150 mA/mm), while G_a shows a rapid increase from 12.8 dB to 18.0 dB and then slightly compromised. The NF_{min} at PGP was determined to be 3.79 dB, which was 2.89 dB higher than the result at I_{DS} = 10 mA/mm. The degradation in NF_{min} with increasing I_{DS} is believed to result from increased high-field diffusion noise and aggravated self-heating effect as the device was working with high drain currents [17], [18]. Fig. 5(d) investigates NF_{min} and G_a at various frequencies. NF_{min} was measured to be only 0.65 dB at 1 GHz, while G_a reached 18.3 dB concurrently. The low NF_{min} is attributed to the low I_G of the device, which is otherwise detrimental to noise performance of the device [9], [18]. Nevertheless, both NF_{min} and G_a degrade as increasing the working frequency (f). In particular, NF_{min} shows a sharp rise beyond 3 GHz and increases to 4.3 dB at 3.5 GHz. Typically, NF_{min} can be expressed in a second-order

TABLE I
COMPARISON OF DEVICE PARAMETERS AND NOISE PERFORMANCE

Param./Ref.	This Work	[7]	[9]	[21]
Structure	***p*-GaN HEMT**	MIS *p*-GaN	GaN HEMT	GaN MIS HEMT
V_{TH} (V)	**2.7**	0.3	< 0	-4
L_G (μm)	**1**	1	0.7	0.25
I_G @ I_{DS} (mA/mm)	**10^{-5} @ 10**	10^{-7} @ 10	10^{-1} @ ~66	10^{-9} @ 300
f_T/f_{MAX} (GHz)	**6.1/10.3**	6.0/9.8	N.A.	43/98
NF_{min} (dB) @ f (GHz)	**0.9 @ 2**	N.A.	~ 0.7 @ 3	~ 0.7 @ 2.5
G_a (dB) @ f (GHz)	**12.8 @ 2**	N.A.	N.A.	~17 @ 3
Γ_S (mag.) @ f (GHz)	**0.83 @ 2**	N.A.	N.A.	N.A.

approximation as [19] and [20]:

$$NF_{min}(f) = 10\log[1 + 2A_1(f/f_T) + 2A_2(f/f_T)^2] \quad (1)$$

where A_1 and A_2 are two coefficients associated with source/gate access resistance and the internal noise source. For relatively low working frequency stage, the second-order term could be truncated. However, as working frequency approaches f_T, the second-order term of $(f/f_T)^2$ has to be taken into account when assessing NF_{min} of the device, resulting in a rapid increase of NF_{min}.

Table I illustrates a comparison between *p*-GaN HEMT and reported results. [7], [9], [21]. With the same L_G of 1 μm as the MIS *p*-GaN HEMT in [7], the device in this work achieves slightly higher f_T/f_{MAX} and acceptably small on-state gate current. The comparison also reveals that the *p*-GaN HEMT in this work demonstrates a similar level of NF_{min} at low frequencies as the HEMT in [9] and the MIS-HEMT in [21], although the *p*-GaN HEMT holds a relatively larger L_G. Additionally, the *p*-GaN HEMT in this work significantly reduces gate leakage current compared to HEMT in [9] and enables the E-mode operation and single polarity power supply. As further scaling down L_G, the *p*-GaN HEMT would expect to exhibit even higher $f_T/f_{MAX}/G_m$ that may further greatly lower NF_{min} at higher frequency, providing new opportunities for the design of LNA circuits and front-end receivers.

IV. CONCLUSION

For LNA applications, RF performance of a *p*-GaN HEMT is thoroughly investigated. The E-mode *p*-GaN HEMT features a low gate current and CMOS-compatible ohmic contacts. The device exhibits V_{TH} of 2.7 V, a small on-state I_G of 16.3 nA/mm, and a breakdown voltage higher than 80 V. In addition to f_T/f_{MAX} of 6.1/10.3 GHz, *p*-GaN HEMT also delivers an IIP3 of 15.8 dBm at 2 GHz, and good frequency immunity of device linearity characteristics. Moreover, outstanding noise performance including a NF_{min} of 0.9 dB and a G_a of 12.8 dB are achieved at 2 GHz. Bias and frequency dependences of NF_{min} and G_a are also investigated. An overall smallest NF_{min} is found to be 0.65 dB at 1 GHz at I_{DS} = 10 mA/mm, while G_a exhibits 18.3 dB concurrently and stays above 10 dB for the frequency range investigated.

ACKNOWLEDGMENT

The authors would like to thank ShanghaiTech Quantum Device Laboratory (SQDL) and Electromechanical Energy and Electronic Devices Testing Platform for providing technical support.

References

[1] W. Song, Z. Zheng, T. Chen, J. Wei, L. Yuan, and K. J. Chen, "RF linearity enhancement of GaN-on-Si HEMTs with a closely coupled double-channel structure," *IEEE Electron Device Lett.*, vol. 42, no. 8, pp. 1116–1119, Aug. 2021, doi: 10.1109/LED.2021.3087785.

[2] J. C. Mayeda, D. Y. C. Lie, and J. Lopez, "A highly efficient 18–40 GHz linear power amplifier in 40-nm GaN for mm-wave 5G," *IEEE Microw. Wireless Compon. Lett.*, vol. 31, no. 8, pp. 1008–1011, Aug. 2021, doi: 10.1109/LMWC.2021.3085241.

[3] P. Neininger, L. John, M. Zink, D. Meder, M. Kuri, A. Tessmann, C. Friesicke, M. Mikulla, R. Quay, and T. Zwick, "Broadband 100-W Ka-band SSPA based on GaN power amplifiers," *IEEE Microw. Wireless Compon. Lett.*, vol. 32, no. 6, pp. 708–711, Jun. 2022, doi: 10.1109/LMWC.2022.3166563.

[4] J. Zhou, H. Guo, Y. Gu, and X. Zou, "Demonstration and modeling of frequency tripler based on GaN Schottky diode pair," *Microelectron. J.*, vol. 125, Jul. 2022, Art. no. 105464, doi: 10.1016/j.mejo.2022.105464.

[5] Y. Gu, W. Huang, Y. Zhang, J. Sui, Y. Wang, H. Guo, J. Zhou, B. Chen, and X. Zou, "Temperature-dependent dynamic performance of p-GaN gate HEMT on Si," *IEEE Trans. Electron Devices*, vol. 69, no. 6, pp. 3302–3309, Jun. 2022, doi: 10.1109/TED.2022.3167342.

[6] J. Chen, W. Huang, H. Qu, Y. Zhang, J. Zhou, B. Chen, and X. Zou, "Study of minority carrier traps in p-GaN gate HEMT by optical deep level transient spectroscopy," *Appl. Phys. Lett.*, vol. 120, no. 21, May 2022, Art. no. 212105, doi: 10.1063/5.0083362.

[7] C.-J. Yu, C.-W. Hsu, M.-C. Wu, W.-C. Hsu, C.-Y. Chuang, and J.-Z. Liu, "Improved DC and RF performance of novel MIS p-GaN-gated HEMTs by gate-all-around structure," *IEEE Electron Device Lett.*, vol. 41, no. 5, pp. 673–676, May 2020, doi: 10.1109/LED.2020.2980584.

[8] Y. Cheng, Y. H. Ng, Z. Zheng, and K. J. Chen, "RF enhancement-mode p-GaN gate HEMT on 200 mm-Si substrates," *IEEE Electron Device Lett.*, vol. 44, no. 1, pp. 29–31, Jan. 2023, doi: 10.1109/LED.2022.3220693.

[9] C. Sanabria, A. Chakraborty, H. Xu, M. J. Rodwell, U. K. Mishra, and R. A. York, "The effect of gate leakage on the noise figure of AlGaN/GaN HEMTs," *IEEE Electron Device Lett.*, vol. 27, no. 1, pp. 19–21, Jan. 2006, doi: 10.1109/LED.2005.860889.

[10] N. Xu, R. Hao, F. Chen, X. Zhang, H. Zhang, P. Zhang, X. Ding, L. Song, G. Yu, K. Cheng, Y. Cai, and B. Zhang, "Gate leakage mechanisms in normally off p-GaN/AlGaN/GaN high electron mobility transistors," *Appl. Phys. Lett.*, vol. 113, no. 15, Oct. 2018, doi: 10.1063/1.5041343.

[11] G. Zhou, Z. Wan, G. Yang, Y. Jiang, R. Sokolovskij, H. Yu, and G. Xia, "Gate leakage suppression and breakdown voltage enhancement in p-GaN HEMTs using metal/graphene gates," *IEEE Trans. Electron Devices*, vol. 67, no. 3, pp. 875–880, Mar. 2020, doi: 10.1109/TED.2020.2968596.

[12] S. Haifeng, A. R. Alt, H. Benedickter, and C. R. Bolognesi, "High-performance 0.1-μm gate AlGaN/GaN HEMTs on silicon with low-noise figure at 20 GHz," *IEEE Electron Device Lett.*, vol. 30, no. 2, pp. 107–109, Feb. 2009, doi: 10.1109/LED.2008.2010339.

[13] Z. Zheng, W. Song, J. Lei, Q. Qian, J. Wei, M. Hua, S. Yang, L. Zhang, and K. J. Chen, "GaN HEMT with convergent channel for low intrinsic knee voltage," *IEEE Electron Device Lett.*, vol. 41, no. 9, pp. 1304–1307, Sep. 2020, doi: 10.1109/LED.2020.3010810.

[14] S. H. Sohel, A. Xie, E. Beam, H. Xue, T. Razzak, S. Bajaj, S. Campbell, D. White, K. Wills, Y. Cao, W. Lu, and S. Rajan, "Improved DC-RF dispersion with epitaxial passivation for high linearity graded AlGaN channel field effect transistors," *Appl. Phys. Exp.*, vol. 13, no. 3, Feb. 2020, Art. no. 036502, doi: 10.35848/1882-0786/ab7480.

[15] Z. H. Liu, G. I. Ng, S. Arulkumaran, Y. K. T. Maung, K. L. Teo, S. C. Foo, and V. Sahmuganathan, "Improved linearity for low-noise applications in 0.25-μm GaN MISHEMTs using ALD Al_2O_3 as gate dielectric," *IEEE Electron Device Lett.*, vol. 31, no. 8, pp. 803–805, Aug. 2010, doi: 10.1109/LED.2010.2051136.

[16] L. F. Tiemeijer, R. J. Havens, R. de Kort, and A. J. Scholten, "Improved Y-factor method for wide-band on-wafer noise-parameter measurements," *IEEE Trans. Microw. Theory Techn.*, vol. 53, no. 9, pp. 2917–2925, Sep. 2005, doi: 10.1109/TMTT.2005.854243.

[17] J.-W. Lee, A. Kuliev, V. Kumar, R. Schwindt, and I. Adesida, "Microwave noise characteristics of AlGaN/GaN HEMTs on SiC substrates for broad-band low-noise amplifiers," *IEEE Microw. Wireless Compon. Lett.*, vol. 14, no. 6, pp. 259–261, Jun. 2004, doi: 10.1109/LMWC.2004.828026.

[18] M. A. Mebarki, R. F. D. Castillo, D. Meledin, E. Sundin, M. Thorsell, N. Rorsman, V. Belitsky, and V. Desmaris, "Noise characterization and modeling of GaN-HEMTs at cryogenic temperatures," *IEEE Trans. Microw. Theory Techn.*, vol. 71, no. 5, pp. 1923–1931, May 2023, doi: 10.1109/TMTT.2022.3226480.

[19] R. A. Pucel, H. A. Haus, and H. Statz, "Signal and noise properties of gallium arsenide microwave field-effect transistors," in *Advances in Electronics and Electron Physics*, vol. 38. New York, NY, USA: Academic Press, 1975, pp. 195–265.

[20] J. Mateos, T. Gonzalez, D. Pardo, S. Bollaert, T. Parenty, and A. Cappy, "Design optimization of AlInAs–GaInAs HEMTs for low-noise applications," *IEEE Trans. Electron Devices*, vol. 51, no. 8, pp. 1228–1233, Aug. 2004, doi: 10.1109/TED.2004.832095.

[21] Z. H. Liu, G. I. Ng, S. Arulkumaran, Y. K. T. Maung, K. L. Teo, S. C. Foo, V. Sahmuganathan, T. Xu, and C. H. Lee, "High microwave-noise performance of AlGaN/GaN MISHEMTs on silicon with Al_2O_3 gate insulator grown by ALD," *IEEE Electron Device Lett.*, vol. 31, no. 2, pp. 96–98, Feb. 2010, doi: 10.1109/LED.2009.2036135.